



LUH-GRACE2018: A New Time Series of Monthly Gravity Field Solutions from GRACE

Igor Koch, Jakob Flury, Majid Naeimi, and Akbar Shabanloui

Abstract

In this contribution, we present the LUH-GRACE2018 time series of monthly gravity field solutions covering the period January 2003–March 2016. The solutions are obtained from GRACE K-Band Range Rate (KBRR) measurements as main observations. The monthly solutions are computed using the in-house developed GRACE-SIGMA software. The processing is based on dynamic orbit and gravity field determination using variational equations and consists of two main steps. In the first step, 3-hourly orbital arcs of the two satellites and the state transition and sensitivity matrices are dynamically integrated using a modified Gauss-Jackson integrator. In this step, initial state vectors and 3D accelerometer bias parameters are adjusted using GRACE Level-1B reduced-dynamic positions as observations. In the second step, normal equations are accumulated and the normalized spherical harmonic coefficients up to degree and order 80 are estimated along with arc-wise initial states, accelerometer biases and empirical KBRR parameters. Here KBRR measurements are used as main observations and reduced-dynamic positions are introduced to solve for the low frequency coefficients. In terms of error degree standard deviations as well as Equivalent Water Heights (EWH), our gravity field solutions agree well with RL05 solutions of CSR, GFZ and JPL.

Keywords

GRACE · Gravity field recovery · Time-variable gravity field · GRACE Follow-On

1 Introduction

In this paper we report on the status of the determination of monthly Earth gravity field models from orbit positions and K-band satellite-to-satellite tracking measurements of the GRACE and GRACE Follow-On (GRACE-FO) low Earth orbiters at Leibniz Universität's Institut für Erdmessung. We give an overview on the processing approach of the LUH-GRACE2018 time series of monthly solutions from GRACE data. We briefly report on the first monthly solutions

from GRACE-FO data that will be described in detail in an upcoming article.

The first batch of the LUH-GRACE2018 time series, covering 7 years (2003–2009), was presented and published in 2018 (Naeimi et al. 2018). In September 2019, a second batch containing monthly solutions from the years 2010 to 2016 was published. The processing approach for the solutions is the method of dynamic orbit and gravity field determination based on the equations of motion, also often referred to as the variational equations approach, e.g. Montenbruck and Gill (2005), Vallado (2013). We implemented it in a compact all-MATLAB program named GRACE-Satellite orbit Integration and Gravity field analysis in MATLAB (GRACE-SIGMA). The code uses strongly vectorized modules for numerical integration of reference orbits and the contributions to the design matrix (state transition matrix,

I. Koch (✉) · J. Flury · M. Naeimi · A. Shabanloui
Institut für Erdmessung, Leibniz Universität Hannover, Hannover,
Germany
e-mail: koch@ife.uni-hannover.de

sensitivity matrix). To allow for the vectorization, a modified Gauss-Jackson numerical integrator was developed. The least-squares parameter estimation is done in a two-step procedure: in the first step, a suitable reference orbit and accelerometer calibration parameters are estimated as a fit to reduced-dynamic orbit positions. In the second step, K-Band Range Rate (KBRR) observations are added to estimate updates to spherical harmonic gravity field coefficients. In order not to constrain the solutions towards the background force models of the pre-adjusted orbits, arc-specific parameters from step 1 are estimated together with the coefficients of the Earth's time-variable potential (Meyer et al. 2015). To allow for an efficient data handling and processing, observations, parameters and force model data are stored and updated in arc-wise data capsules.

The implementation of the force effects was validated in comparison with computation results from other GRACE ACs within the new COmbination Service for Time-variable Gravity solutions (COST-G) (Meyer et al. 2018). It must be noted that we used RL05 Atmosphere and Ocean De-aliasing (AOD) models to correct for rapid mass variations, as our processing started before the more recent and more accurate RL06 AOD models were available. Also, we used RL02 Level-1B data products as the reprocessed RL03 Level-1B data were not yet available for the first batch of our processing. For the GRACE-FO gravity field solutions RL06 AOD models and RL04 data products were used. For a future time series of monthly GRACE solutions, we plan to use updated data and models.

The LUH-GRACE2018 monthly solutions were in principle estimated up to spherical harmonic degree and order 80. The monthly parameter estimation was done by stacking normal equations from orbital arcs of 3 h each; initial satellite state corrections, 3-axes accelerometer instrument biases and empirical range-rate corrections were estimated arc-wise. Our current stochastic model uses uniform weights for the reduced-dynamic orbit position pseudo-observations on the one hand and the K-band range-rate observations on the other.

Obtained results are compared to the solutions of other ACs in terms of error degree standard deviations that show the level of time-variable signal, modeling errors and random measurement errors with respect to a long-term reference model. In addition, obtained results are compared to those of other ACs in terms of mass variation time series for selected geophysical processes. This evaluation shows that for most months the quality of our results is similar to results from other ACs. For some months with poorer and more heterogeneous data quality, we have obtained a similar quality level by estimating spherical harmonic parameters up to degree 60 only. For other months with an even more difficult data situation, the results are not yet satisfactory and therefore not yet published.

One of the future goals of our group is to test how inhomogeneous data quality as seen, e.g., in post-fit range-rate residuals, propagates in the gravity recovery processing. We expect that changes in the parametrization or modifications of the input sensor data can help to identify and disentangle some of the involved effects.

2 Overview of the Gravity Field Recovery Method

Here, we mention the main elements of dynamic orbit and gravity field determination from GRACE and GRACE-FO sensor data. A paper with more details on our implementation is in preparation. We refer to Fig. 1 for a generalized overview. As the problem is highly nonlinear, a reference orbit that closely matches the true orbit (represented by the GRACE Level-1B data products) is determined using dynamic orbit integration from a priori force models. Then reduced observations are computed. After the linearization, the reduced observations are used to estimate parameter updates.

Orbit integration is based on the equations of motion

$$\ddot{\mathbf{r}} = -\frac{GM_{\oplus}}{r^3}\mathbf{r} + \ddot{\mathbf{r}}_p \quad (1)$$

with the central (Keplerian) term and a sum of accelerations due to perturbing forces $\ddot{\mathbf{r}}_p$. The perturbing forces include the higher harmonics of the time-variable gravity field, direct and indirect tidal forces, forces from non-tidal mass redistribution, and non-gravitational forces acting on the satellites.

The reference orbit is obtained by numerically integrating the first order ordinary differential equations

$$\left. \begin{aligned} \dot{\mathbf{r}} &= \mathbf{v} \\ \dot{\mathbf{v}} &= -\frac{GM_{\oplus}}{r^3}\mathbf{r} + \ddot{\mathbf{r}}_p \end{aligned} \right\}. \quad (2)$$

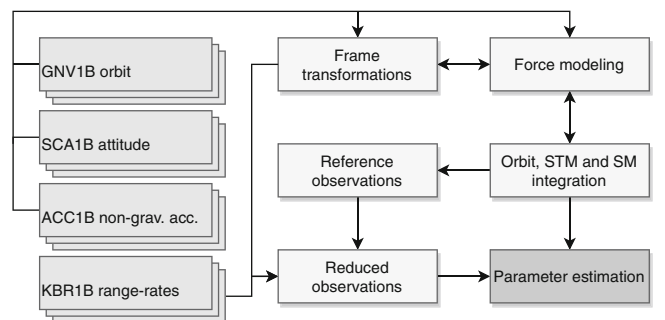


Fig. 1 Simplified procedure of gravity field recovery from satellite-to-satellite tracking data with the variational equations approach. STM: state transition matrix, SM: sensitivity matrix, non-grav. acc: non-gravitational acceleration

For the non-gravitational forces, the accelerometer observations of each satellite are used, considering bias and scale calibration parameters. For the perturbing forces, frame transformations between geocentric and inertial frames or between satellite body frames and inertial frame need to be applied; for the latter, star camera based attitude data are used.

In the first estimation step, the orbit is iteratively fitted to orbit positions from a reduced-dynamic orbit as pseudo-observations, in order to ensure a sufficiently good linearization for the second estimation step. The partial derivatives in the design matrix of the estimation require the integration of the state transition and sensitivity matrices along with the orbit integration. In the second step, K-band range-rate observations are added, and updates to spherical harmonic coefficients are introduced as main unknown parameters.

3 Data

For the GRACE processing, we used the Level-1B data products of the release 2 (RL02) (Case et al. 2010). These data products include K-band range-rate observations (KBR1B), reduced-dynamic positions and velocities (GNV1B), accelerometer measurements representing the non-gravitational accelerations (ACC1B) and satellite attitude (SCA1B). All quantities of the Level-1B data products were used with 5 s sampling during numerical integration. For K-band range-rates, light-time and antenna offset corrections from the KBR1B data products were included. In the processing the standard GNV1B reduced-dynamic orbit positions were used as pseudo-observations. We assume that they allow for a sufficiently good linearization in the first estimation step. Nevertheless, the influence of the orbit type and their characteristics, e.g. dynamic information in reduced-dynamic orbits or high frequency noise in kinematic orbits, on the recovered gravity field solutions may deserve further systematic investigations in the future.

4 Force Modeling

Force models needed for the numerical integration of the satellite trajectory and the state transition and sensitivity matrices are summarized in Table 1. The force models consider gravitational effects of tidal and non-tidal nature as well as non-gravitational effects. The non-gravitational effects are measured by the onboard accelerometers and have to be corrected for scale factors and biases during processing. Except for the acceleration due to the Earth's gravity potential and the non-gravitational acceleration, all effects were pre-computed using the GNV1B reduced-dynamic orbits and were not altered during numerical orbit integration. We

Table 1 Force models applied for the LUH-GRACE2018 time series of monthly gravity field solutions. *d/o*: indicates the utilized maximum degree/order of the spherical harmonic coefficients

| Force | Models and parameters |
|------------------------|------------------------------------|
| Gravity field | GIF48 (<i>d/o</i> : 300) [1] |
| Direct tides | Moon, Sun (DE405) [2] |
| Solid Earth tides | IERS Conventions 2010 [3] |
| Ocean tides | EOT11a (<i>d/o</i> : 80) [4], [5] |
| Relativistic effects | IERS Conventions 2010 [3] |
| Solid earth pole tides | IERS Conventions 2010 [3] |
| Ocean pole tides | IERS Conventions 2010 [3], [6] |
| De-aliasing | AOD1B RL05 (<i>d/o</i> : 100) [7] |
| Non-gravitational | ACC1B [8] |

References: [1]: Ries et al. (2011), [2]: Standish (1998), [3]: Petit and Luzum (2010), [4]: Savchenko and Bosch (2012), [5]: Rieser et al. (2012), [6]: Desai (2002), [7]: Dobslaw et al. (2013), [8]: Case et al. (2010)

assume that future releases of the LUH-GRACE monthly gravity field solutions will benefit from updated ocean tide models such as FES2014 (Carrere et al. 2015) and from the AOD1B RL06 de-aliasing products (Dobslaw et al. 2017).

5 Numerical Integration

An accurate numerical integration of the satellite orbits and the state transition and sensitivity matrices can be regarded as the most time-consuming processing part of gravity field recovery. In order to save computational time while ensuring an integration accuracy suitable for gravity field recovery, we developed a modified version of the widely used predictor-corrector Gauss-Jackson integrator, e.g. Berry and Healy (2004), Montenbruck and Gill (2005), Vallado (2013). The impact of the corrector step on a GRACE-like orbit (near circular with an eccentricity of 0.001 and an altitude of about 500 km) was validated for different integration orders and step sizes. For the typical GRACE integration step size of 5 s and the integration order of 8, the impact of the corrector step is in the order of 10^{-13} m for the position and 10^{-13} m/s for the velocity and thus can be neglected (Naeimi 2018). However, the corrector formulas can be used to simplify the formulation of the predictor step considerably, allowing a straightforward, vectorized and thus efficient implementation. While more details of this integration technique will be covered in an upcoming publication, the modified Gauss-Jackson equations and ancillary sets of coefficients needed for an implementation can be found below. The modified Gauss-Jackson equations for state prediction have the following form:

$$\left. \begin{aligned} \mathbf{r}_{i+1} &= \mathbf{r}_i + h\dot{\mathbf{r}}_i + h^2\mathbf{pBA} \\ \dot{\mathbf{r}}_{i+1} &= \dot{\mathbf{r}}_i + h\mathbf{qBA} \end{aligned} \right\} \quad (3)$$

Table 2 Parameters $p_j = \delta_{j+1} - \gamma_j^* - \delta_{j+1}^*$ and $q_j = \gamma_j - \gamma_j^*$ for the numerical integration with the modified Gauss-Jackson integrator

| | | | | | | |
|-------|-------------------------|-----------------------|----------------------------|----------------------|-----------------------|---------------------|
| j | 0 | 1 | 2 | 3 | 4 | 5 |
| p_j | 0 | $\frac{1}{2}$ | $\frac{1}{6}$ | $\frac{1}{8}$ | $\frac{19}{180}$ | $\frac{3}{32}$ |
| q_j | 0 | 1 | $\frac{1}{2}$ | $\frac{5}{12}$ | $\frac{3}{8}$ | $\frac{251}{720}$ |
| j | 6 | 7 | 8 | 9 | 10 | 11 |
| p_j | $\frac{33953}{453600}$ | $\frac{8183}{115200}$ | $\frac{3250433}{47900160}$ | $\frac{4671}{71680}$ | $\frac{275}{3456}$ | $\frac{863}{10080}$ |
| q_j | $\frac{110397}{362880}$ | $\frac{8183}{115200}$ | $\frac{3250433}{47900160}$ | $\frac{4671}{71680}$ | $\frac{19087}{60480}$ | $\frac{665}{2016}$ |

These coefficients can be obtained from the Adams-Bashforth coefficients γ_j , the Adams-Moulton coefficients γ_j^* and Stoermer and Cowell coefficients δ_j, δ_j^*

where $\mathbf{r}_{i+1}, \dot{\mathbf{r}}_{i+1}$ (row vectors) are the predicted position and velocity vectors; \mathbf{r}_i and $\dot{\mathbf{r}}_i$ (row vectors) are the position and velocity vectors at a current time and h is the integration step size. \mathbf{pBA} and \mathbf{qBA} represent the summation parts of the integrator, where the specific integration order is considered. For the computation of the results presented in this study an integration order of 12 was used. In the modified version of the Gauss-Jackson integrator this integration order corresponds to a summation over indices $j = [1, m]$ where m is the integration order decreased by one. The row vectors \mathbf{p} and \mathbf{q} contain the coefficients p_j and q_j that are defined in Table 2. Matrix \mathbf{A} contains row-wise the acceleration vector at the current time stamp i as well as the accelerations of $m - 1$ back points. The result of multiplying matrix \mathbf{B} with matrix \mathbf{A} are the acceleration backward differences up to order $m - 1$. The entries of matrix \mathbf{B} are summarized in Table 3. For initialization a Runge-Kutta integrator of order 4 is used.

6 Parametrization

The parametrization chosen for the two-step approach is summarized in Table 4. The main idea behind the two-

Table 4 Specifics of the two-step approach applied for the LUH-GRACE2018 time series of monthly gravity field solutions

| | |
|--|---|
| <i>Step 1: Orbit pre-adjustment</i> | |
| Arc length | 3 h |
| Numerical integrator | Modified Gauss-Jackson |
| Integration step size | 5 s |
| Observations | GNV1B positions (5 s) |
| Weighting | Identity matrix |
| Local parameters | Initial state, acc. biases |
| Global parameters | No |
| Constraints | Not applied |
| Regularization | Not applied |
| <i>Step 2: Orbit adjustment and gravity field recovery</i> | |
| Arc length | 3 h |
| Numerical integrator | Modified Gauss-Jackson |
| Integration step size | 5 s |
| Observations | GNV1B positions (30 s) K-band range-rates (5 s) |
| Weighting | GNV1B positions $\sigma_0 = 0.02$ m KBRR $\sigma_0 = 2 \times 10^{-7}$ m/s |
| Local parameters | Initial state, acc. biases, empirical KBRR parameters |
| Global parameters | Spherical harmonic coefficients up to degree and order 80 (60) |
| Constraints | Not applied |
| Regularization | Not applied |

step approach is to reduce the number of iterations during gravity field recovery and therefore to save computational time. This is achieved by estimating appropriate a priori values for the initial satellite states as well as accelerometer calibration parameters using only reduced-dynamic orbit positions as observations in the orbit pre-adjustment (Wang et al. 2015). For this release of monthly gravity field solutions the accelerometer biases are estimated arc-wise while the scale factors are held fixed to a priori values reported in Bettadpur (2009). The satellite orbits are parametrized by an arc length of 3 h. The aim of this arc length is to allow a more precise orbit fit to observations, as inaccuracies, e.g. in force modeling, can be balanced by the very frequent estimation of local arc parameters. Compared to the usual

Table 3 Entries of the matrix \mathbf{B} for the vectorized computation of backward differences

| | | | | | | | | | | |
|---|-----|----|------|-----|------|-----|------|----|-----|---|
| 1 | 0 | 0 | 0 | 0 | 0 | 0 | 0 | 0 | 0 | 0 |
| 1 | -1 | 0 | 0 | 0 | 0 | 0 | 0 | 0 | 0 | 0 |
| 1 | -2 | 1 | 0 | 0 | 0 | 0 | 0 | 0 | 0 | 0 |
| 1 | -3 | 3 | -1 | 0 | 0 | 0 | 0 | 0 | 0 | 0 |
| 1 | -4 | 6 | -4 | 1 | 0 | 0 | 0 | 0 | 0 | 0 |
| 1 | -5 | 10 | -10 | 5 | -1 | 0 | 0 | 0 | 0 | 0 |
| 1 | -6 | 15 | -20 | 15 | -6 | 1 | 0 | 0 | 0 | 0 |
| 1 | -7 | 21 | -35 | 35 | -21 | 7 | -1 | 0 | 0 | 0 |
| 1 | -8 | 28 | -56 | 70 | -56 | 28 | -8 | 1 | 0 | 0 |
| 1 | -9 | 36 | -84 | 126 | -126 | 84 | -36 | 9 | -1 | 0 |
| 1 | -10 | 45 | -120 | 210 | -252 | 210 | -120 | 45 | -10 | 1 |

arc length of one day, no constrained dynamic empirical parameters, such as cycle per revolution accelerations or more frequent stochastic parameters, have to be co-estimated in order to achieve a good orbit fit. In the second step the K-band range-rates are used as main observations, along with reduced-dynamic positions. As additional unknowns, kinematic empirical KBRR parameters are introduced. In total 8 empirical parameters consisting of bias and bias-rates as well as periodic bias and bias-rates are estimated per arc (Kim 2000). We solve for the bias and bias-rates every 90 min and for periodic bias and bias-rates every 180 min. Range-rates and reduced-dynamic orbit positions are combined on normal equation level using a technique-specific weighting. The spherical harmonic coefficients of the Earth's gravity potential are obtained together with the arc-specific parameters without any constraints, regularizations or stochastic accelerations. The number of parameters to be estimated in the second step of the procedure equals 6557 global parameters representing the normalized spherical harmonic coefficients of the Earth's potential (for maximum degree 80) as well as 6448 arc-specific parameters if 31 days of observations are considered.

7 GRACE-FO Solutions

In Sect. 8 we will jointly evaluate the LUH-GRACE2018 gravity field solutions (2003–2016) as well as first GRACE-FO results (June 2018–August 2019). For the GRACE-FO results a slightly modified processing strategy was applied. The most recent de-aliasing product AOD1B RL06 (Dobslaw et al. 2017) up to degree and order 180 was used. In addition, atmospheric tides were considered according to Biancale and Bode (2006). Accelerometer scale factors were estimated arc-wise along with the biases. The Earth's gravity potential was estimated up to degree and order 96.

8 Results and Evaluation

The convergence of exemplary gravity field solutions in terms of the error degree standard deviation for March 2006 (good ground track coverage) and September 2004 (sparse ground track coverage) are shown in Fig. 2. Arcs with a length of 3 h are stacked successively, overall leading to a decrease of the error degree standard deviations of the corresponding solutions. Figure 2a, b shows the convergence from the beginning, highlighting the rapid convergence during the first seven days. For the remainder of a month, the convergence rate is much slower as can be seen in Fig. 2c, d. The results demonstrate that satisfactory sub-monthly

gravity field solutions of the time-variable Earth's gravity potential can often be obtained without any constraints, regularizations or a priori information such as solutions from previous months or weeks. Note that the convergence rate can vary significantly depending on sensor data quality and distribution of ground tracks.

The computed monthly gravity field solutions are compared to the solutions of the three official ACs: CSR (Center for Space Research, The University of Texas at Austin), GFZ (German Research Centre for Geosciences) and JPL (Jet Propulsion Laboratory, California Institute of Technology). Since we used AOD1B RL05 products for the correction of rapid mass variations, our solutions are compared to the RL05 previous generation solutions, in order to allow for a fair comparison. The reference solutions CSR RL05 (Bettadpur 2012), GFZ RL05a (Dahle et al. 2012) and JPL RL05 (Watkins and Yuan 2014) are obtained from the International Centre for Global Earth Models (ICGEM) (Ince et al. 2019).

Error degree standard deviations of the monthly solutions are illustrated in Fig. 4. The mean error degree standard deviations are computed for the two periods 2003–2009 and 2010–2016 separately. As a reference field the recent static gravity field model GOCO06s (Kvas et al. 2019) was subtracted from the solutions of all 4 ACs. It can be seen that in general the noise characteristics of the solutions are similar, not considering degree 2. In general the amplitudes of the LUH error degree standard deviations are slightly larger when compared to the other ACs. Degree 4 for both periods as well as degree 3 for the second period show larger error degree standard deviations indicating a larger noise for these degrees. A comparison on the coefficients level showed that the degree 4 deviation is caused by the \overline{C}_{44} and \overline{S}_{44} coefficients. We presume that this deviation is caused by the applied parametrization, since the mean error degree standard deviations of about one year of GRACE-FO processing with a slightly changed parametrization does not show any significant deviations in the low degrees. Nevertheless, further investigations are needed. Error degree standard deviations show effects of orbital resonances (Cheng and Ries 2017) near degrees 31 and 46. The orbital resonance near degree 62 is missing in the second period leading to a smaller noise for the higher degrees 62–80 compared to period 1.

A comparison of exemplary global maps of mass variations in terms of Equivalent Water Height (EWH) can be seen in Fig. 3. Global maps based on CSR RL05 and the LUH-GRACE2018 solutions for every second month of the year 2008 are shown with respect to the static model GOCO06s. The \overline{C}_{20} coefficients of all solutions were replaced by values obtained from Satellite Laser Ranging (SLR) (Cheng and

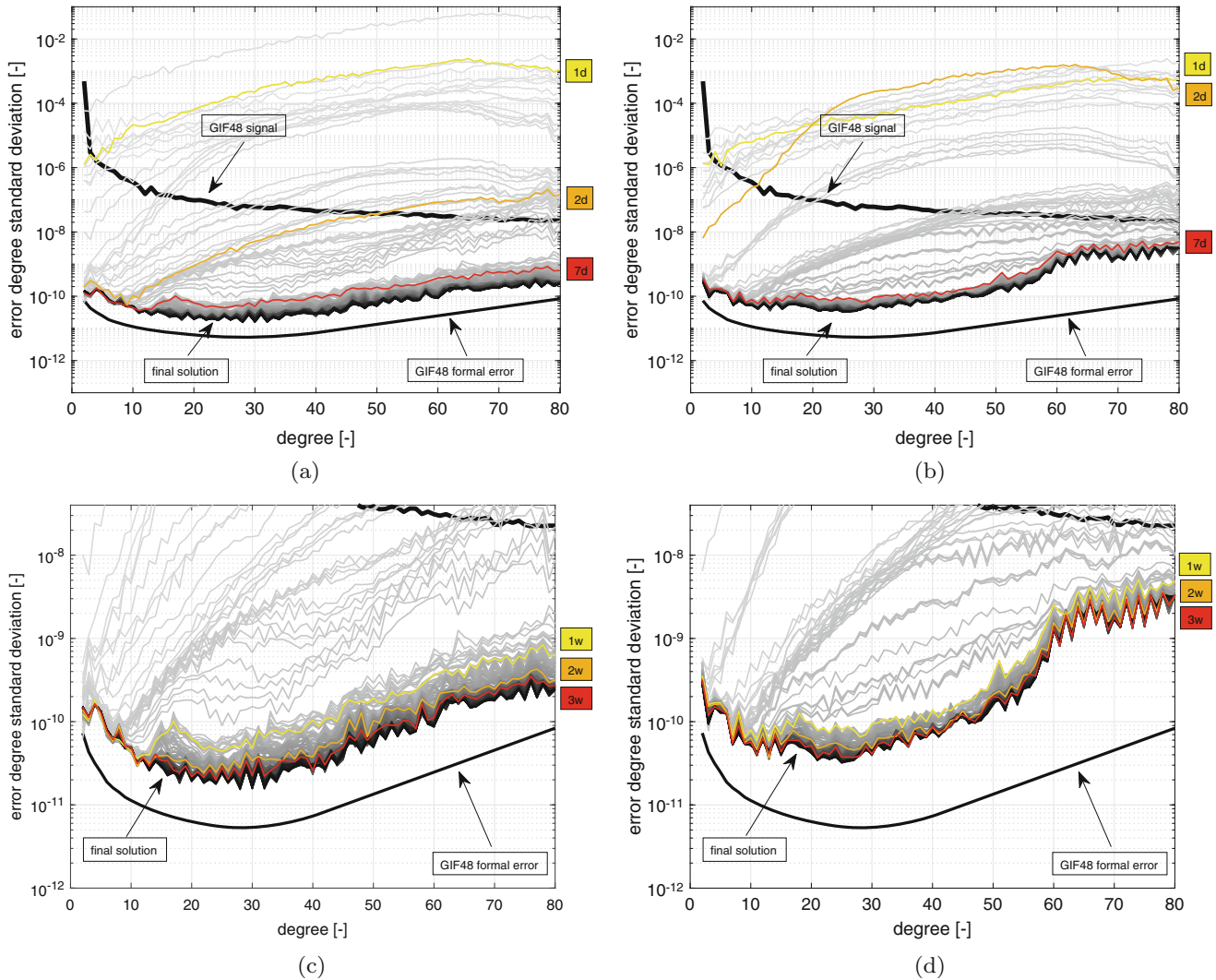


Fig. 2 Exemplary successive stacking of 3 hourly orbital arcs and the error degree standard deviations of the corresponding gravity field solution for March 2006 (good ground track coverage) and September 2004 (sparse ground track coverage) with respect to the gravity field

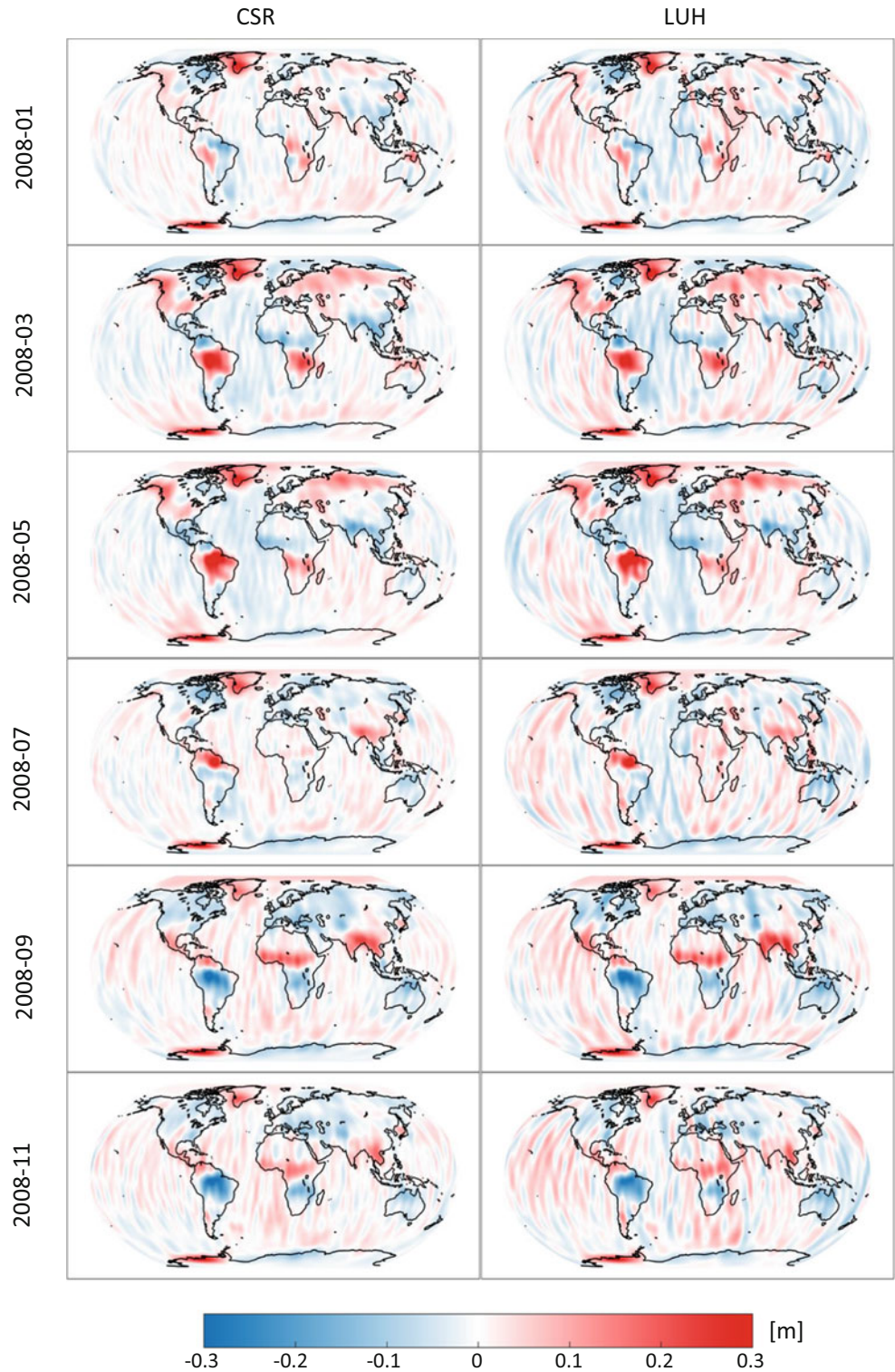
model GIF48. The error degree standard deviations for 1 day, 2 days, 7 days, 2 weeks and 3 weeks of observation data are highlighted. (a) March 2006. (b) September 2004. (c) March 2006 zoom. (d) September 2004 zoom

Ries 2017). In order to mitigate the meridional North-South stripes, the spherical harmonic coefficients differences were smoothed using the Gaussian filter (Wahr et al. 1998) with a half width of 400 km before computing the EWH. It can be seen that larger mass variations such as in the Amazon region, central Africa, India, Southeast Asia, Greenland and Northeast Canada can be localized equally well in both CSR and LUH solutions. The meridional stripes in the LUH maps

are slightly stronger, which is consistent with the slightly higher error degree standard deviations in Fig. 4, and their characteristics suggest differences in the analysis noise that should be further studied.

Exemplary Equivalent Water Height time series for Greenland and the Amazon and Ganges basins based on the same processing as applied for the global EWH maps are shown in Fig. 5. The time series cover the GRACE period and

Fig. 3 Global Equivalent Water Height (EWH) for every second month of the year 2008. Left side: CSR RL05 solutions; right side: LUH solutions. The C_{20} coefficients were replaced by SLR values in all solutions. As a reference model the static gravity field model GOCO06s (reference epoch: 2010-01-01) was subtracted. The spherical harmonic coefficients differences were smoothed using the Gaussian filter with a half width of 400 km



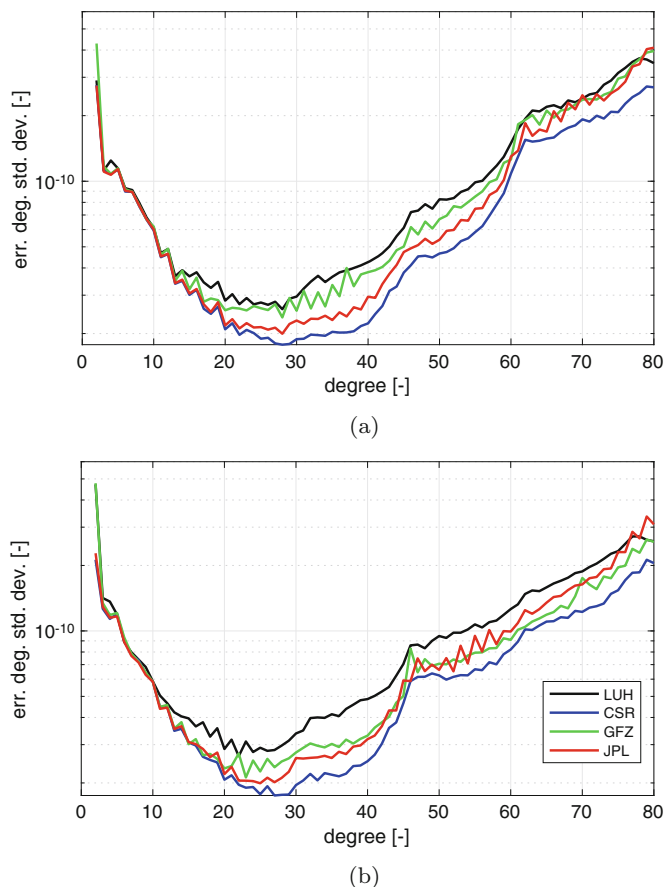


Fig. 4 Mean of error degree standard deviations of the four analysis centers for degrees 2–80 with respect to the static model GOCO06s. The solutions were divided into two periods: 2003–2009 (a) and 2010–2016 (b). The \bar{C}_{20} coefficients were not replaced. All solutions are zero-tide. A specific month is considered when a solution from all 4 centers is available. We define a monthly solution as a solution that is based on satellite data from one calendar month, i.e. solutions combining sensor data of neighboring months are not considered. Periods when regularizations were applied are excluded

additionally include the first available GRACE-FO solutions. The EWH signals of all four ACs covering a time span of more than 16 years show a high degree of consistency for all three regions. This indicates that the signal content of the four ACs' solutions does not exhibit large differences. The degradation of the GRACE sensor data manifests as gaps in the second half of the time series.

Acknowledgements We are thankful for the valuable comments of the two anonymous reviewers who helped to improve the manuscript considerably. Part of this work was funded by Deutsche Forschungsgemeinschaft (DFG) (SFB1128 geo-Q: Collaborative Research Centre 1128 "Relativistic Geodesy and Gravimetry with Quantum Sensors").

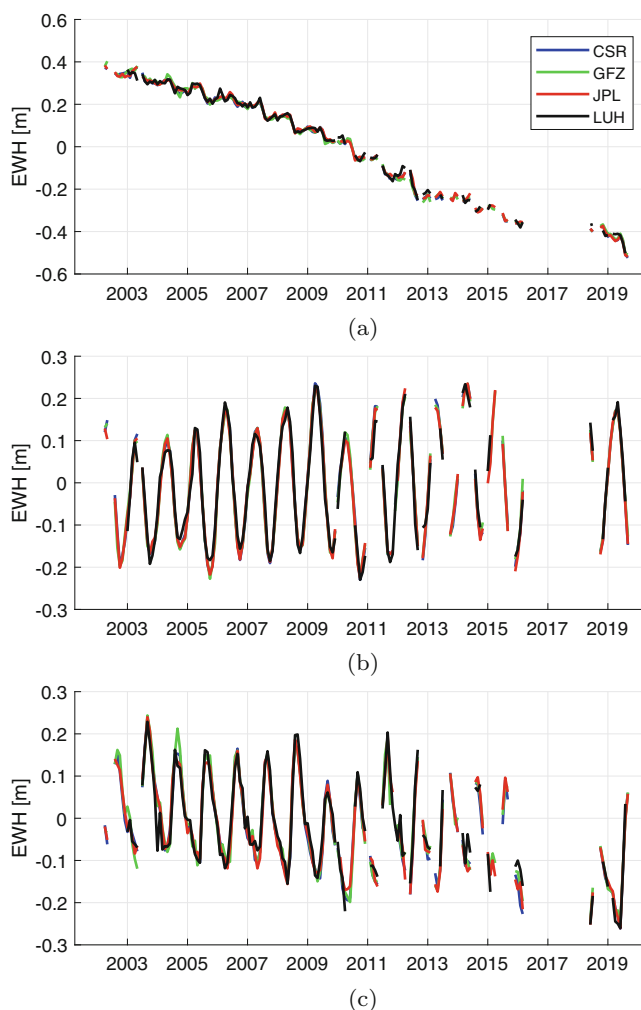


Fig. 5 Equivalent Water Heights (EWH) in three regions: (a) Greenland, (b) Amazon basin, (c) Ganges basin. EWH values are region mean values. The \bar{C}_{20} coefficients in all solutions were replaced by SLR values. As a reference model the static gravity field model GOCO06s (reference epoch: 2010-01-01) was subtracted. The spherical harmonic coefficients differences were smoothed using the Gaussian filter with a half width of 400 km

References

- Berry MM, Healy LM (2004) Implementation of Gauss-Jackson integration for orbit propagation. *J Astronaut Sci* 52(3):331–357
- Bettadpur S (2009) Recommendation for a-priori bias & scale parameters for level-1B acc data (version 2), GRACE TN-02. Technical note. Center for Space Research, The University of Texas at Austin
- Bettadpur S (2012) UTCSR level-2 processing standards document for level-2 product release 0005. Technical report GRACE, 327–742. Center for Space Research, The University of Texas at Austin

- Biancale R, Bode A (2006) Mean annual and seasonal atmospheric tide models based on 3-hourly and 6-hourly ECMWF surface pressure data. Scientific technical report STR06/01. GeoForschungsZentrum Potsdam, Germany
- Carrere L, Lyard F, Cancet M, Guillot A (2015) FES2014, a new tidal model on the global ocean with enhanced accuracy in shallow seas and in the Arctic region. *Geophys Res Abstr*, EGU2015-5481. EGU General Assembly 2015, Vienna, Austria
- Case K, Kruizinga G, Wu S-C (2010) GRACE Level 1B data product user handbook (JPL D-22027), Technical report. Jet Propulsion Laboratory, California Institute of Technology, Pasadena, CA, USA
- Cheng MK, Ries JC (2017) The unexpected signal in GRACE estimates of C20. *J Geod* 91(8):897–914. <https://doi.org/10.1007/s00190-016-0995-5>
- Dahle C, Flechtner F, Gruber C, König D, König R, Michalak G, Neumayer, K-H (2012) GFZ GRACE level-2 processing standards document for level-2 product release 0005: revised edition, January 2013, (Scientific Technical Report STR - Data ; 12/02 rev. ed.), Deutsches GeoForschungsZentrum GFZ, 21 p. <http://doi.org/10.2312/GFZ.b103-1202-25>
- Desai SD (2002) Observing the pole tide with satellite altimetry. *J Geophys Res* 107(C11). <https://doi.org/10.1029/2001JC001224>
- Dobslaw H, Bergmann-Wolf I, Dill R, Poropat L, Thomas M, Dahle C, Esselborn S, König R, Flechtner F (2017) A new high-resolution model of non-tidal atmosphere and ocean mass variability for de-aliasing of satellite gravity observations: AOD1B RL06. *Geophys J Int* 211(1):263–269. <https://doi.org/10.1093/gji/ggx302>
- Dobslaw H, Flechtner F, Bergmann-Wolf I, Dahle C, Dill R, Esselborn S, Sasgen I, Thomas M (2013) Simulating high-frequency atmosphere-ocean mass variability for de-aliasing of satellite gravity observations: AOD1B RL05. *J Geophys Res Oceans* 118:3704–3711. <https://doi.org/10.1002/jgrc.20271>
- Ince ES, Barthelmes F, Reißland S, Elger K, Förste C, Flechtner F, Schuh H (2019) ICGEM – 15 years of successful collection and distribution of global gravitational models, associated services and future plans. *Earth Syst Sci Data* 11:647–674. <http://doi.org/10.5194/essd-11-647-2019>
- Kim J (2000) Simulation study of a low-low satellite-to-satellite tracking mission, PhD thesis, The University of Texas at Austin
- Kvas A, Mayer-Gürr T, Krauß S, Brockmann JM, Schubert T, Schuh W-D, Pail R, Gruber T, Meyer U, Jäggi A (2019) The satellite-only gravity field model GOCO06s. EGU General Assembly 2019, 7.-12. April 2019, Vienna, Austria. <https://doi.org/10.13140/RG.2.2.14101.99047>
- Meyer U, Jäggi A, Beutler G, Bock H (2015) The impact of common versus separate estimation of orbit parameters on GRACE gravity field solutions. *J Geod* 89(7):685–696. <https://doi.org/10.1007/s00190-015-0807-3>
- Meyer U, Jenny B, Dahle C, Flechtner F, Save H, Bettadpur S, Landerer F, Boening C, Kvas A, Mayer-Gürr T, Lemoine JM, Bruinsma S, Jäggi A (2018) COST-G: The new international combination service for time-variable gravity field solutions of the IAG/IGFS. GRACE/GRACE-FO Science Team Meeting 2018, 9.-11. October 2018, Potsdam, Germany
- Montenbruck O, Gill E (2005) *Satellite orbits – Models, Methods and Applications*, 3rd edn., Springer, Berlin, Germany, ISBN: 978-3-642-58352-0. <http://doi.org/10.1007/978-3-642-58351-3>
- Naemi M (2018) A modified Gauss-Jackson method for the numerical integration of the variational equations. EGU General Assembly 2018, 8.-13. April 2018, Vienna, Austria
- Naemi M, Koch I, Khami A, Flury J (2018) IfE monthly gravity field solutions using the variational equations. EGU General Assembly 2018, 8.-13. April 2018, Vienna, Austria. <https://doi.org/10.15488/4452>
- Petit G, Luzum B. (2010) IERS Conventions (2010), IERS Technical Note No. 36. Verlag des Bundesamts für Kartographie, Frankfurt am Main, Germany
- Ries JC, Bettadpur S, Poole S, Richter T (2011) Mean Background Gravity Fields for GRACE Processing. GRACE Science Team Meeting 2011, 8.-10. August 2011, Austin, TX, USA
- Rieser D, Mayer-Gürr T, Savchenko R, Bosch W, Wunsch J, Dahle C, Flechtner F (2012) The ocean tide model EOT11a in spherical harmonics representation. Technical note
- Savchenko R, Bosch W (2012) EOT11a - empirical ocean tide model from multi-mission satellite altimetry. DGFI Report No. 89, Deutsches Geodätisches Forschungsinstitut (DGFI), München, Germany
- Standish EM (1998) JPL planetary and lunar ephemerides, DE405/LE405 (JPL Iteroffice Memorandum IOM 312.F-98-048)
- Vallado DA (2013) *Fundamentals of astrodynamics and applications*, 4th edn. Microcosm Press, Hawthorne, CA, USA, ISBN: 978-188188318-0
- Wahr J, Molenaar M, Bryan F (1998) Time variability of the Earth's gravity field: Hydrological and oceanic effects and their possible detection using GRACE. *J Geophys Res* 103(B12):30205–30229. <https://doi.org/10.1029/98JB02844>
- Wang C, Xu H, Zhong M, Feng W (2015) Monthly gravity field recovery from GRACE orbits and K-band measurements using variational equations approach. *Geodesy Geodynamics* 6(4):253–260. <https://doi.org/10.1016/j.geog.2015.05.010>
- Watkins MM, Yuan D (2014) JPL level-2 processing standards document for level-2 product release 05.1. Technical report GRACE, 327–744, Jet Propulsion Laboratory, California Institute of Technology, Pasadena, CA, USA

Open Access This chapter is licensed under the terms of the Creative Commons Attribution 4.0 International License (<http://creativecommons.org/licenses/by/4.0/>), which permits use, sharing, adaptation, distribution and reproduction in any medium or format, as long as you give appropriate credit to the original author(s) and the source, provide a link to the Creative Commons licence and indicate if changes were made.

The images or other third party material in this chapter are included in the chapter's Creative Commons licence, unless indicated otherwise in a credit line to the material. If material is not included in the chapter's Creative Commons licence and your intended use is not permitted by statutory regulation or exceeds the permitted use, you will need to obtain permission directly from the copyright holder.

